

# Highly Selective Terahertz Bandpass Filters Based on Trapped Mode Excitation

Oliver Paul,<sup>1,\*</sup> René Beigang,<sup>1,2</sup> and Marco Rahm<sup>1,2</sup>

<sup>1</sup>*Department of Physics and Research Center OPTIMAS, University of Kaiserslautern, Germany*

<sup>2</sup>*Fraunhofer Institute for Physical Measurement Techniques IPM, Freiburg, Germany*

We present two types of metamaterial-based spectral bandpass filters for the terahertz (THz) frequency range. The metamaterials are specifically designed to operate for waves at normal incidence and to be independent of the field polarization. The functional structures are embedded in films of benzocyclobutene (BCB) resulting in large-area, free-standing and flexible membranes with low intrinsic loss. The proposed filters are investigated by THz time-domain spectroscopy and show a pronounced transmission peak with over 80% amplitude transmission in the passband and a transmission rejection down to the noise level in the stopbands. The measurements are supported by numerical simulations which evidence that the high transmission response is related to the excitation of trapped modes.

PACS numbers: 42.79.-e; 42.79.Ci; 07.57.Hm; 42.70.-a

## I. INTRODUCTION

In the last ten years, metamaterials have emerged to be powerful tools for the manipulation of light on the subwavelength scale. The scientific interest has been primarily driven by the possibility of creating materials with new electromagnetic properties not occurring in nature such as e. g. negative index materials [1, 2], invisibility cloaks and transformation optics [3, 4]. However, metamaterials are not only of scientific interest for their exotic properties. In the frequency range between 0.1 and 10 THz, which is usually referred to as the THz gap, the lack of electromagnetic response of most natural materials has substantially obstructed the development of functional components. For the THz technology, metamaterials can play a crucial role for the conception of artificial optical components since their electromagnetic properties can be exactly designed to match the functionality of an envisioned optical component. In this context, several optical elements as e. g. wave plates [5], THz amplitude [6] and phase modulators [7] and spatial modulators [8] have already been successfully demonstrated. Recently, the excitation of so-called trapped modes, i.e. modes that are weakly coupled to an external electromagnetic field, has been observed in metamaterials [9, 10, 11, 12, 13]. These modes show analogies to the electromagnetically induced transparency (EIT) of atomic systems [14, 15] like a sharp phase dispersion of the transmitted radiation and a narrow transmission band within a broad stopband. Such properties open the possibility for the construction of very efficient and compact metamaterial-based bandpass filters with a high selectivity.

In this paper, we present two types of spectral bandpass filters for the THz frequency range based on the excitation of trapped modes. The corresponding resonances of the subwavelength elements have been optimized to obtain a high transmission in the passband and

an efficient suppression of transmitted radiation in the stopbands. The two implemented metamaterial designs are a cross-slot structure and a wire-and-plate structure (see Figs. 1(a) and 1(b)). Such structures have been originally introduced in the microwave regime [16, 17]. They operate at normal incidence and are independent of the polarization of the incident light. The polarization insensitivity is a direct consequence of the 4-fold rotational symmetry of the structure [18]. In order to enhance the bandpass effect we employed a multilayer technique to embed several functional layers in films of BCB. The BCB serves as a homogeneous background matrix and enables us to fabricate large-area, free-standing and flexible metamaterial membranes. This is especially important with regard to a practical integration of such metamaterial components in THz systems since the beam diameter of THz radiation is usually in the order of several millimeters. The designed and fabricated bandpass filters were experimentally characterized by means of THz time-domain spectroscopy.

## II. FILTER DESIGN UND FABRICATION

The cross-slot structure is set-up by an array of 3  $\mu\text{m}$  wide cross-shaped slots (Fig. 1(a)). The enclosed crosses are formed by 46  $\mu\text{m}$  long and 9  $\mu\text{m}$  wide cross bars. The cross bars act as small electric dipoles that can be excited by an incident THz wave. The lattice constants of the structure are 68  $\mu\text{m}$  in the x- and y-direction and 40  $\mu\text{m}$  in the z-direction. In contrast, the wire-and-plate structure (Fig. 1(b)) is composed by two separated layers being 9.5  $\mu\text{m}$  apart from each other. The front layer consists of a two-dimensional wire grid formed by 17  $\mu\text{m}$  wide wires whereas the background layer is represented by an array of square plates with a side length of 50  $\mu\text{m}$ . The lattice constants for this structure are 60  $\mu\text{m}$  in the x- and y-direction and 35  $\mu\text{m}$  in the z-direction. Since the adjacent edges of each two plates act as a capacitor whereas the facing strip of the wire grid acts as an inductor, the composite structure forms an LC-resonant

---

\*Electronic address: paul@physik.uni-kl.de

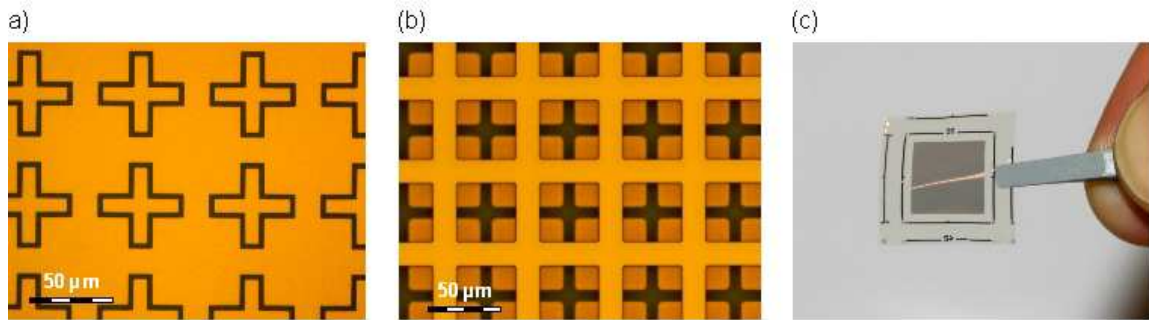


Fig. 1: Microscope pictures of (a) the cross-slot structure and (b) the two layers of wire-and-plate structure. (c) Resulting metamaterial membrane with a functional area of  $9 \times 9 \text{ mm}^2$ .

circuit that can be excited by a normally incident THz wave.

The fabrication of the metamaterial films was performed in a multilayer process with alternating layers of BCB 3022-63 and copper on top of a silicon substrate. The BCB layers were fabricated by a spin coating technique followed by a thermal curing process in a vacuum oven at  $300^\circ\text{C}$  for about 5 h. The metal layers were patterned by standard UV-lithography using an AZ nLof 2035 photoresist, an EVG 620 mask aligner and an electron beam evaporation of 200 nm copper. For the plate-and-wire design a strict alignment of the plates and wires layers within a unit cell is necessary to ensure the functionality of the structure. For this purpose we used alignment marks providing an accuracy in the order of  $1 \mu\text{m}$ . A microscope image of one layer of unit cells of both designs is shown in Figs. 1(a) and 1(b), respectively. The films were then removed from the silicon substrate in a 30% solution of KOH. The resulting free-standing membranes are  $17 \times 17 \text{ mm}^2$  large, mechanically and chemically stable and quite flexible. A photograph of the resulting membrane is presented in Fig. 1(c).

We fabricated membranes with one layer of unit cells of the cross-slot structure and two layers of unit cells of the wire-and-plate structure. However, as shown in [19], the free-standing membranes can be stacked on top of another to further increase the number of layers. Similar to the double-cross structure reported in [19], the structures used for the filter designs are independent of the polarization and the coupling between the functional metal layers in neighboring membranes can be neglected due to the thick BCB spacer. Hence, the alignment of individual membranes is not crucial to the orientation or the relative position of the membranes and can be performed under simple visual control.

### III. RESULTS AND DISCUSSION

The transmission characteristics of the metamaterial filters was analyzed by standard THz time-domain spectroscopy with a detectable frequency range of 0.1 –

2.5 THz and a frequency resolution of 9 GHz. The THz radiation was linearly polarized and was focused under normal incidence on the sample surface to a spot size of 1.5 mm. Finally, the measured transmission spectra have been normalized by a reference spectrum without sample to obtain the amplitude transmittance of the filters.

We analyzed one and two layers of unit cells of the cross-slot structure by measuring a single and two stacked membranes, each fabricated with one layer of unit cells. For the wire-and-plate structure we analyzed two and four layers of unit cells by using a single and two stacked membranes where each membrane consisted of two layers of unit cells. The experimentally obtained spectral transmission data were compared to numerical simulations which have been carried out by a commercially available time-domain solver (CST Microwave Studio), where the BCB can be described by a dielectric constant of  $\epsilon = 2.67$  and a loss parameter of  $\tan \delta = 0.01$  [19]. However, we varied the permittivity of BCB in order to fit the numerical data to the experimental results and obtained reasonable agreement by using  $\epsilon = 2.45$  for the cross-slot and  $\epsilon = 1.85$  for the wire-and-plate design.

Figs. 2(a) and 2(b) show the spectral amplitude transmission and reflection of the cross-slot-structure and the wire-and-plate structure, respectively. The experimental transmission results (colored solid lines) are in good agreement with the numerical simulations (colored dashed lines). Both filter designs reveal a pronounced passband around 1.3 THz. As expected, the frequency selectivity of the bandpass filters increases with increasing number of layers of unit cells. For two layers of the cross-slot structure and for four layers of the wire-and-plate structure the FWHM bandwidth of the passband is  $\Delta f = 0.3 \text{ THz}$  in each case. Both filters offer a very high amplitude transmission over 80%, a fast roll-off and a very efficient blocking in the lower and upper rejection bands down to the noise level where the incident radiation is almost completely reflected. Moreover, the transmission response of the cross-slot structure is ripple-free, whereas the wire-and-plate filter exhibits a faster roll-off.

The origin of these strong resonances can be attributed

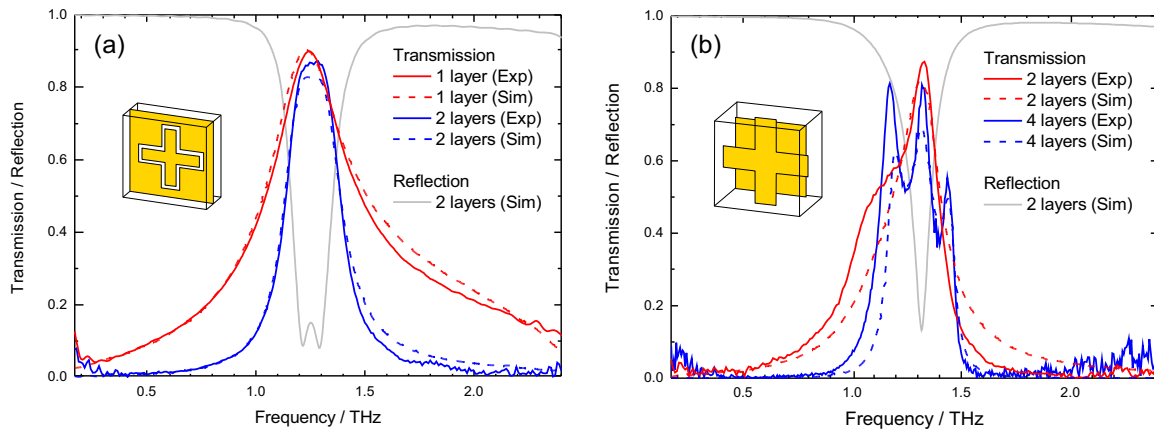


Fig. 2: Experimental (Exp) and numerical (Sim) amplitude transmission and reflection results for (a) the cross-slot and (b) the wire-and-plate structure for different numbers of layers of unit cells.

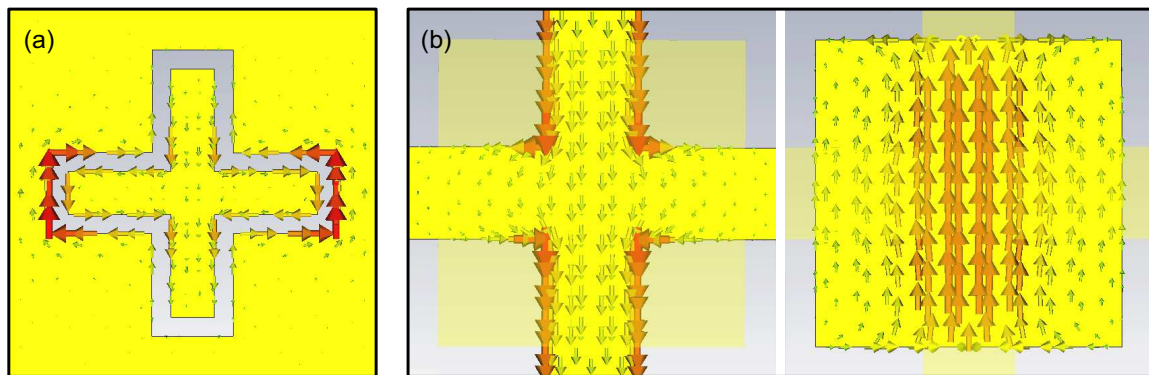


Fig. 3: Surface current distribution at the center frequency of the passband for (a) the cross-slot structure and (b) the front plane (left) and the backplane (right) of the wire-and-plate structure. The incident electric field is vertically polarized.

to so-called trapped modes [9, 10, 11, 12, 13], i.e. modes that are weakly coupled to electromagnetic waves incident from free space. For such modes the radiation losses are very small in comparison to the stored field energy which leads to an enhanced transmission at the resonance frequency. The excitation of trapped modes is evidenced by the simulation of the surface current distribution in the metamaterial structures presented in Fig. 3. At the resonance frequency, the induced currents are counter propagating at distinct sections of the structure with almost similar magnitude. As a consequence, the resulting dipole moment and therefore the dipolar coupling to external electromagnetic fields is strongly reduced which results in a high transmission of electromagnetic radiation through the metamaterial structure at frequencies near the resonance.

In particular, for the cross-slot structure the surface currents are counter propagating at the two opposing edges of the slot (Fig. 3(a)). This specific current distribution is related to the fact that the outer metal frame is just the complementary of a cross structure which causes

the driven currents to oscillate with opposite phase. For the wire-and-plate structure, it's the currents in the front layer (metal wire grid) and the background layer (square metal patches) that are in opposite phase (Fig. 3(b)). This can be explained by the different functions of the layers in the equivalent LC-resonant circuit. As mentioned in Sec. 2, the plates act as capacitors, i.e. the phase of the driven currents is shifted by  $+\pi/2$  with respect to the external electric field, whereas the wires act as inductors which causes a phase shift of  $-\pi/2$ . This implies that the excited currents in the two layers must be opposite in phase.

#### IV. EFFECTIVE MATERIAL PARAMETERS

For a more quantitative characterization of the investigated metamaterial bandpass filters, we further applied a retrieval algorithm [20] to calculate the effective values of the refractive index  $n$  and the permittivity  $\epsilon$  from the simulated transmission and reflection data. The retrieval

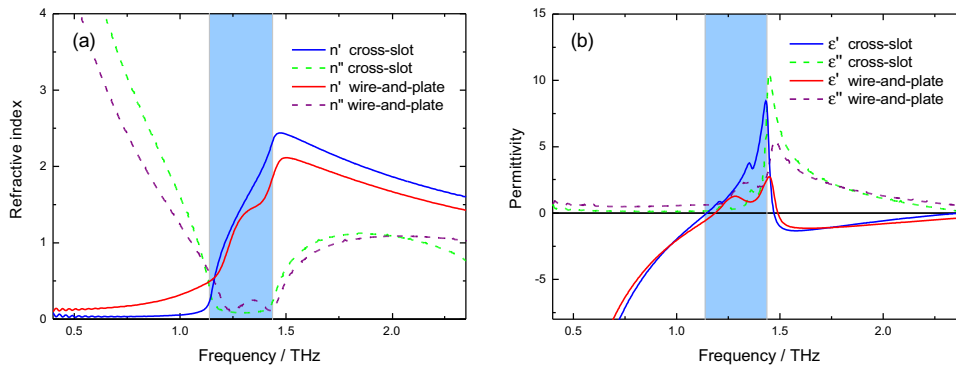


Fig. 4: Retrieved values of (a) the effective index of refraction and (b) the effective permittivity of the bandpass filters where  $(\cdot)'$  and  $(\cdot)''$  denote the real and imaginary part, respectively. The spectral passband is shaded.

was supported by additional computation of the phase advance of a propagating plane wave across the material to ensure that the correct branch of the refractive index was chosen.

The resulting effective refractive index and the permittivity are plotted in Fig. 4 for both the cross-slot structure and the wire-and-plate structure. Thereby,  $(\cdot)'$  and  $(\cdot)''$  denote the real and imaginary part, respectively and the spectral passband is indicated by a blue box. It can be seen from Fig. 4(b) that the permittivity of both structures exhibits a characteristic narrow resonance, where  $\epsilon'$  is only positive in the vicinity of the resonance frequency. As a consequence, only in this region  $n''$  is sufficiently small to allow high transmission leading to the observed passband. It should be noted that both structures exhibit similar effective material parameters even though their constituent elements widely differ in shape and geometry. This is due to the fact, that the transmission response of both structures is related to the same origin: the excitation of trapped modes in subwavelength elements. Moreover, since the quality factors of the excited resonances are equal, the media that are composed by the two structures are equivalent in the framework of effective medium theory. Another remarkable result is the rapid increase of  $n'$  within the passband as displayed in Fig. 4(a). This strong frequency dispersion leads to an increase of the group index which is given by  $n_g = \frac{c}{v_g} = c \frac{\partial k'}{\partial \omega} = n' + \frac{\partial n'}{\partial \omega} \omega$  with the group velocity  $v_g$  and the dispersion relation  $k' = n' \frac{\omega}{c}$ . From the plotted curves for  $n'$ , the average group index can be calculated in the passband to be  $n_g = 7.4$  for the wire-and-plate structure and even  $n_g = 9.3$  for cross-slot structure. This means that a propagating pulse whose spectrum covers the passband will be transmitted with a significant time delay. Although the group refractive index is not as high as can be expected in the case of

electromagnetically induced transparency [15] or accordingly plasmon-induced transparency [10] where a dark mode is phase-coupled to a broadband dipole resonance, the calculations demonstrate the highly dispersive character of trapped mode excitation.

## V. CONCLUSION

In summary, we have presented two types of metamaterial bandpass filters in the THz frequency range. The implemented metamaterials are based on a cross-slot and a wire-and-plate structure, respectively. The filters are embedded in membranes of BCB allowing free-standing, flexible films and are designed to operate at normal incidence and to be independent of the polarization of the incident light. We have shown that the observed transmission response is related to the excitation of trapped modes where the reduced coupling to the electromagnetic field leads to an enhanced transmission at the resonance frequency.

The special characteristics of the presented filters is an outstanding high transmission over 80% in the passband and a fast roll-off down to the noise level in the stopbands. The spectral bandwidth of the realized band-pass filters is 0.3 THz. Such highly selective filters can be used to remove unwanted transmitted signals in pre-defined frequency bands and have potential applications in the field of THz diagnostics.

We thank Dr. Christian Imhof from the Department of Electrical and Computer Engineering, University of Kaiserslautern, for supportive comments and discussions, and the Nano+Bio Center at the University of Kaiserslautern for their support in the sample fabrication.

[1] V. D. Veselago, “The electrodynamics of substances with simultaneously negative values of  $\epsilon$  and  $\mu$ ,” Soviet

- [2] D. R. Smith, W. J. Padilla, D. C. Vier, S. C. Nemat-Nasser, and S. Schultz, "Composite Medium with Simultaneously Negative Permeability and Permittivity," *Phys. Rev. Lett.* **84**, 4184–4187 (2000).
- [3] J. B. Pendry, D. Schurig, and D. R. Smith, "Controlling Electromagnetic Fields," *Science* **312**, 1780–1782 (2006).
- [4] J. Li and J. B. Pendry, "Hiding under the Carpet: A New Strategy for Cloaking," *Phys. Rev. Lett.* **101**, 203,901 (2008).
- [5] A. C. Strikwerda, K. Fan, H. Tao, D. V. Pilon, X. Zhang, and R. D. Averitt, "Comparison of birefringent electric split-ring resonator and meanderline structures as quarter-wave plates at terahertz frequencies," *Opt. Express* **17**(1), 136–149 (2009).
- [6] W. J. Padilla, H.-T. Chen, J. Zide, A. Gossard, A. Taylor, and R. Averitt, "Active terahertz metamaterial devices," *Nature* **444**, 597 (2006).
- [7] H.-T. Chen, W. J. Padilla, M. J. Cich, A. K. Azad, R. D. Averitt, and A. J. Taylor, "A metamaterial solid-state terahertz phase modulator," *Nature Photon.* **3**, 148 (2009).
- [8] W. L. Chan, H.-T. Chen, A. J. Taylor, I. Brener, M. J. Cich, and D. M. Mittleman, "A spatial light modulator for terahertz beams," *Appl. Phys. Lett.* **94**, 213,511 (2009).
- [9] V. A. Fedotov, M. Rose, S. L. Prosvirnin, N. Papasimakis, and N. I. Zheludev, "Sharp Trapped-Mode Resonances in Planar Metamaterials with a Broken Structural Symmetry," *Phys. Rev. Lett.* **99**, 147,401 (2007).
- [10] S. Zhang, D. A. Genov, Y. Wang, M. Liu, and X. Zhang, "Plasmon-Induced Transparency in Metamaterials," *Phys. Rev. Lett.* **101**, 047,401 (2008).
- [11] N. Papasimakis, V. A. Fedotov, S. L. Prosvirnin, and N. I. Zheludev, "Metamaterial Analog of Electromagnetically Induced Transparency," *Phys. Rev. Lett.* **101**, 253,903 (2008).
- [12] P. Tassin, L. Zhang, T. Koschny, E. N. Economou, and C. M. Soukoulis, "Low-Loss Metamaterials Based on Classical Electromagnetically Induced Transparency," *Phys. Rev. Lett.* **102**, 053,901 (2009).
- [13] N. Liu, L. Langguth, T. Weiss, J. Kaestel, M. Fleischhauer, T. Pfau, and H. Giessen, "Plasmonic analogue of electromagnetically induced transparency at the Drude damping limit," *Nat. Mater.* **8**, 758–762 (2009).
- [14] S. E. Harris, J. E. Field, and A. Imamoglu, "Nonlinear optical processes using electromagnetically induced transparency," *Phys. Rev. Lett.* **64**, 1107–1110 (1990).
- [15] C. Liu, Z. Dutton, C. H. Behroozi, and L. V. Hau, "Observation of coherent optical information storage in an atomic medium using halted light pulses," *Nature* **409**, 490–493 (2001).
- [16] B. A. Munk, *Frequency Selective Surfaces: Theory and Design*. (New York: Wiley-Interscience, 2000).
- [17] N. Behdad and K. Sarabandi, "A Frequency Selective Surface With Miniaturized Elements," *IEEE Transactions on Antennas and Propagation* **55**(5), 1239–1245 (2007).
- [18] A. Mackay, "Proof of polarisation independence and nonexistence of crosspolar terms for targets presenting  $n$ -fold ( $n > 2$ ) rotational symmetry with special reference to frequency-selective surfaces," *Electron. Lett.* **25**(24), 1624–1625 (1989).
- [19] O. Paul, C. Imhof, B. Reinhard, R. Zengerle, and R. Beigang, "Negative index bulk metamaterial at terahertz frequencies," *Opt. Express* **16**(9), 6736–6744 (2008).
- [20] X. Chen, T. M. Grzegorzcyk, B.-I. Wu, J. Pacheco, Jr., and J. A. Kong, "Robust method to retrieve the constitutive effective parameters of metamaterials," *Phys. Rev. E* **70**, 016,608 (2004).